

On the Temporal Effects of Mobile Blockers in Urban Millimeter-Wave Cellular Scenarios

Margarita Gapeyenko[†], Andrey Samuylov[†], Mikhail Gerasimenko[†], Dmitri Moltchanov[†], Sarabjot Singh^{*}, Mustafa Riza Akdeniz^{*}, Ehsan Aryafar^{*}, Nageen Himayat^{*}, Sergey Andreev[†], and Yevgeni Koucheryavy[†]

[†]W.I.N.T.E.R. Group, Tampere University of Technology, Tampere, Finland

^{*}Intel Corporation, Santa Clara, CA, USA.

Abstract—User-side performance in millimeter-wave (mmWave) cellular systems is known to be severely affected by blockage of the line-of-sight (LoS) propagation path. In contrast to microwave systems, at shorter mmWave wavelengths such blockage can be caused by human bodies while their mobility within the environment makes the wireless channel alternate between the blocked and non-blocked LoS states. Following recent 3GPP requirements on the *dynamic blockage* as well as the *temporal consistency* of the channel at mmWave frequencies, we in this paper develop a new model for predicting the state of a user in a field of mobile blockers for two representative 3GPP scenarios: urban micro cell (UMi) street canyon and park/stadium/square. We demonstrate that the blockage effects produce an *alternating renewal process* with the exponentially distributed non-blocked intervals and blocked durations that follow the general distribution. We thus derive (i) the mean and the fraction of time spent in blocked/non-blocked state, (ii) the residual blocked/non-blocked time, as well as (iii) the time-dependent conditional probability of having blockage/no blockage at t_1 given that there was blockage/no blockage at time t_0 . The latter is a function of arrival intensity, width, and height of moving blockers, distance to the mmWave access point (AP) as well as heights of the AP and the user device. Our proposed model can be applied in system-level characterization of mmWave cellular communications technology with either analytical or simulation-based methods. In particular, we report on the optimal height and the maximum coverage radius of the mmWave APs while satisfying the target mean data rate constraint. Our supportive system-level simulations corroborate that the use of the proposed formulation allows to considerably decrease the overall *modeling complexity*.

Index Terms—Cellular networks, mmWave frequencies, human body blockage, temporal consistency, mobility of blockers, dynamic blockage.

I. INTRODUCTION

The rapidly growing variety of mobile devices as well as the associated increase in mobile traffic call for the unprecedented improvement in the access data rates at the air interface. To meet more stringent performance requirements, the use of the so-called cellular millimeter-wave (mmWave) technology operating at 28GHz and 72GHz frequencies has been proposed in fifth-generation (5G) mobile systems [1]–[3].

Together with the phenomenal access rates promised by this emerging mmWave technology, the use of extremely high frequency (EHF) band brings along novel unique challenges for wireless system design. One of the crucial aspects along these lines is that having the line-of-sight (LoS) propagation path between a transmitter and a receiver becomes even more

important as compared to the legacy microwave systems. This is because the signal power contributed by reflections and scattering off the objects is significantly smaller [4], [5].

In microwave systems, the objects that may affect the propagation of radio waves are relatively large, and the properties of the radio channel can thus be abstracted away with the generic propagation models ratified by 3GPP, such as the distance dependent formulations in [6]. Following a similar approach, a number of channel models for mmWave cellular systems have recently been developed [7]–[11]. However, in stark contrast to microwave systems, for mmWave technology with its operating wavelength of under a centimeter, the propagation characteristics are impacted not only by larger objects, such as buildings, but also by much smaller obstacles, including cars, lampposts, and even humans. Given that the deployment of future mmWave systems is envisioned in urban squares and streets, 3GPP has identified humans as one of the major factors affecting the mmWave propagation [7]–[9].

The performance of mobile communications systems is typically assessed by employing system-level simulation (SLS) frameworks [12], [13]. Modeling the path loss with simple power-law abstractions, these SLS tools may take into account the necessary details of the target technologies and deliver their output results within a reasonable time. However, when conducting system-level evaluations of the mmWave systems, in addition to the path loss model that captures the propagation environment one needs to explicitly represent and track all of the relevant static and mobile objects across the deployment. Since their dimensions are starting from several centimeters, this requires significant computation resources and thus extends the simulation times.

Motivated by the new effects in mmWave communications systems as well as by the recent 3GPP requirements for 5G channel modeling, this paper studies the *dynamic blockage* caused by humans in outdoor urban mmWave cellular deployments while specifically concentrating on the *temporal consistency* of the link states for a static user.

A. Background and Related Work

The importance of dynamic blockage on the LoS path between the communicating entities in mmWave deployments has recently been manifested to be one of the critical design factors that affects system performance [7]–[9]. An example illustration of the measured path gain experienced by a node in realistic crowded environments is reproduced in Fig. 1 as a

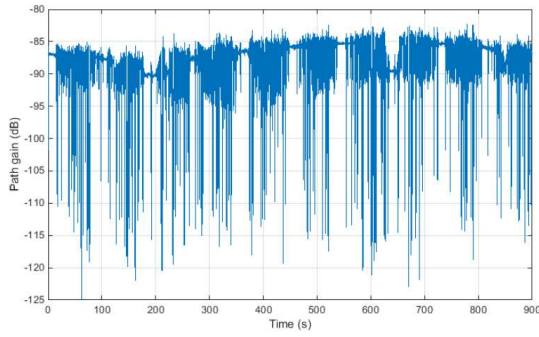


Fig. 1. Path gain in presence of dynamic blockage, reproduced from [14].

function of time. As one may observe, dynamic blockage by small mobile objects within the environment, such as moving people, introduces additional uncertainty in the channel, which may eventually result in sharp drops (up to $30 \sim 40$ dB) in the received signal strength. The timescale of interest as well as the magnitude of these fluctuations are related to the quality of the mmWave system performance.

In wireless communications, the challenge of LoS blockage analysis has first been addressed as part of the studies on urban microwave systems, see e.g., [15], [16]. However, those important results may not be directly applicable for mmWave communications as the objects of interest in mmWave and microwave systems are of fundamentally different nature and hence require dissimilar models for their accurate representation. Indeed, in addition to mobility of smaller obstacles, such as humans, one needs to take into account their inherently random dimensions.

The LoS blockage by humans in mmWave systems has been evaluated with simulation studies in [17]. In [18], a LoS blockage model where humans are represented as cylinders of random width and height was proposed. However, there the authors assumed that both the users and the blockers are stationary. In addition to academic work, the 3GPP community are currently exploring various options for appropriately modeling the phenomenon in question. The latest 3GPP results on the human body blockage characterization have recently been reported in [14], [19].

In [8], the human body blockage is taken into account by creating rectangular screens dropped onto the simulation map. A similar approach is adopted by [20], [21], where the authors also evaluated the accuracy of their methods. Due to the properties of the said propagation model, which generates a random sample of the propagation path at each run, a particular attention of the 3GPP work groups is being paid to spatial and temporal consistency of the mmWave links [8], [19].

In [22], the authors contributed a model for temporal correlation of interference in a mobile network with a certain density of users. It was demonstrated that the correlated propagation states across the users significantly impact the temporal interference statistics. Analytically tractable models for correlated outdoor and indoor shadowing have been proposed in [23] and [24], thus accentuating the high correlation between the locations of the nodes and the shadowing effects.

Even though there has been a considerable literature coverage on user mobility in general [25], [26], to the best of

our knowledge there are only a few studies that incorporate the user mobility into analytically tractable models [27], [28]. These latest results confirm the presence of memory in the LoS blockage process and highlight its dependence on the mobility characteristics of the users.

B. State-of-the-Art and Our Contributions

The goal of this paper is to contribute a novel mathematical methodology that aims to characterize the dynamics and the temporal correlation of LoS human body blockage statistics. In this work, we first propose a model of the LoS blockage for a stationary user in a moving field of blockers. This scenario is more typical for outdoor mmWave communications as compared to stationary blockage considerations addressed in past studies. The blockers are modeled as cylinders of a certain height and width that enter the LoS zone of a mmWave receiver according to a Poisson process in time.

Our proposed analysis is based on the combined application of stochastic geometry, renewal process theory, and queuing models. We address three different scenarios that represent real-life situations, including two street canyon use cases and a park scenario (see Fig. 2). The metrics of interest are those reflecting temporal behavior of the LoS blockage process, such as the mean and the fraction of blocked/non-blocked LoS, the residual time in blocked/non-blocked states, and the time-dependent effects of conditional blocked/non-blocked state probabilities.

In a nutshell, the main contributions of this paper are as follows.

- To analyze the temporal correlation and the dynamic blockage process by human bodies at mmWave frequencies, a novel mathematical model is proposed. It is shown that our analytical expression could be utilized to replace explicit simulation of the mobile blockers in the SLS studies. The associated improvement in the simulation times depends on the crowd intensity and may reach several orders of magnitude.
- To capture the general structure of the dynamic LoS blockage process, including the impact of mobile obstacles, the corresponding mathematical methodology is developed. It is observed that non-blocked/blocked periods form an *alternating renewal process* where the non-blocked intervals follow an exponential distribution and the blocked intervals have a general distribution. The latter is captured by employing methods for the busy period analysis in the $M/GI/\infty$ queuing model.
- To characterize the *temporally consistent* human body blockage process, a simplified approach is developed to calculate the conditional probabilities. It is demonstrated that for the realistic values of the input parameters in all the considered scenarios there always is a significant dependence between the states of the user at t_0 and t_1 over the small timescales.
- To demonstrate the applicability of the proposed methodology, we estimate the optimal height of the mmWave AP that maximizes the average time in non-blocked LoS conditions as well as determine the maximum coverage radius that satisfies a certain target mean data rate.

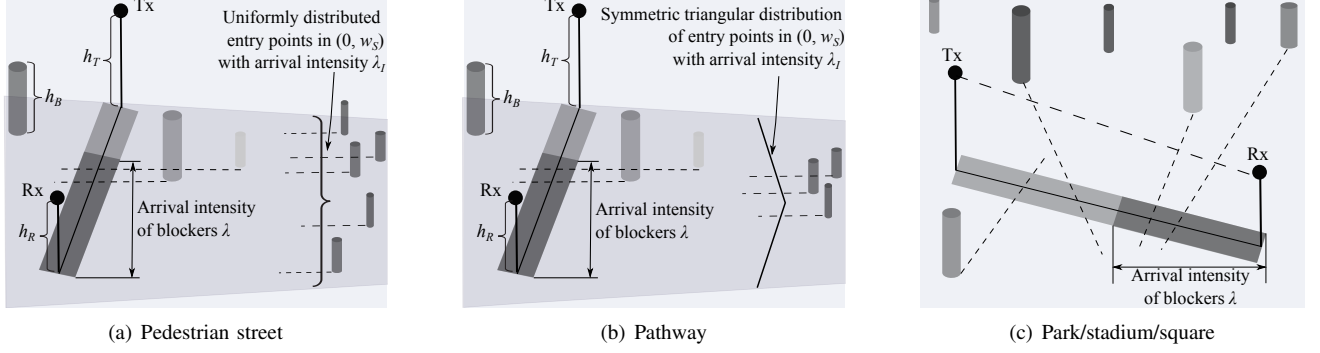


Fig. 2. Three considered scenarios for our analytical modeling.

The rest of this text is organized as follows. In Section II, we introduce our system model and describe the outdoor scenarios proposed by 3GPP, which reflect the real-life mmWave system usage situations. Our analysis for the performance metrics of interest is summarized in Section III. The numerical results, particularly those related to the temporal dependencies in the LoS blockage process, are discussed in Section IV. Section V elaborates on the applications of the proposed methodology. Conclusions are drawn in the last section of the paper.

II. CONSIDERED SYSTEM MODEL

A. General Considerations

Our proposed system model is illustrated in Fig. 2. The transmitter (Tx) and the receiver (Rx) are deployed at the heights of h_T and h_R from the ground, respectively. The distance between the Tx and Rx is r_0 . Following [29], the potential blockers (i.e., humans) are modeled as cylinders with the height of h_B and the base diameter of d_m .

Note that there is always an area between Tx and Rx, where the emergence of a blocker will cause occlusion of the mmWave LoS link. With the above parameters, this area may be approximated by a rectangular shape, named here the *LoS blockage zone* and denoted as $ABCD$ in Fig. 3. The particular dimensions of this area, its geometrical shape, and the position with respect to Tx and Rx can be estimated given the aforementioned parameters as discussed in what follows.

We assume that the speed of blockers V is constant. However, the actual mobility model of blockers depends on the scenario as introduced below. The main parameters and the description of employed notation are collected in Table I.

B. Blocker Mobility and Arrival Modeling

To characterize the human mobility, we consider the following three scenarios:

- *Pedestrian street*. In this case, the mmWave Tx (the AP) is assumed to be mounted on the wall of a building while the Rx may reside at any location on the street of width w_S within the coverage area of the mmWave AP. The blockers move along the straight line parallel to each other and the side of the street at a constant speed of V while their y-coordinates of crossing the width of the street are distributed uniformly within $(0, w_S)$, see Fig. 2(a). The arrival process of blockers appearing on a

vertical line – the width of the street w_S – is Poisson in time with the arrival intensity λ_I .

- *Pathway*. This scenario is similar to the previous case, except for how the blocker positions are distributed in the street. In practice, the users tend to move closer to the center of the walkway. We therefore model their y-coordinates of crossing the width of the street by employing a symmetric triangular distribution over $(0, w_S)$, see Fig. 2(b). The arrival process of blockers crossing the width of the street is again Poisson in time with the arrival intensity λ_I of blockers per time unit.
- *Park/Stadium/Square*. In this scenario, the users are allowed to enter and leave the mmWave LoS blockage zone at any point along the three sides of a rectangle,

TABLE I
SUMMARY OF NOTATION AND PARAMETERS

Notation	Description
h_T, h_R, h_B	Height of Tx, Rx, blockers
r_0	Distance between the bases of Tx and Rx
d_m, V	Diameter and speed of blockers
w_S	Width of the street
w_E, r	Effective width and length of LoS blockage zone
λ_I	Initial arrival intensity of blockers per time unit
λ	Arrival intensity of blockers entering the LoS blockage zone per time unit
λ_S	Arrival intensity of blockers entering the unit area of LoS blockage zone
λ_N	Density of users per unit area
y_A, y_B, y_C, y_D	y-coordinates of the edges of the LoS blockage zone
α	Angle between Y-axis and the segment Tx-Rx
L	Distance walked by a blocker in LoS blockage zone
T	Residence time of a blocker in LoS blockage zone
ω_j, η_j	The non-blocked and blocked time interval
$F_\omega(x), E[\omega]$	CDF, the mean of non-blocked time interval
$F_\eta(x), E[\eta]$	CDF, the mean of blocked time interval
$F_T(x), f_T(x), E[T]$	CDF, pdf, the mean of LoS zone residence time
$F_Y(x)$	CDF of the y-coordinate of blocker entry point
$F_Y^-(x)$	Truncated distribution of the entry point defined on $y_A \leq x \leq y_C$
F_L, f_L	CDF and pdf of the residence distance L
$E[T_i], E[T_n]$	Fraction of time in non-blocked/blocked states
$F_{t_\omega}(x), F_{t_\eta}(x)$	Residual time in non-blocked/blocked states
ξ_j	j^{th} time interval equal to $\omega_j + \eta_j$
$F_\xi(x), f_\xi(x), E[\xi]$	CDF, pdf, the mean of $\omega_j + \eta_j$
$f(x)$	pdf of renewal process
p_{00}, p_{01}	Conditional probabilities to be in non-blocked/blocked states at time t_1 (0 and 1) given that there was non-blocked state at t_0
p_{10}, p_{11}	Conditional probabilities to be in non-blocked/blocked states at time t_1 (0 and 1) given that there was blocked state at t_0

see Fig. 2(c). We assume that both the entry and the exit points are distributed uniformly over the side lengths for each individual user. The arrival process of users into the *LoS blockage zone* is Poisson with the arrival intensity of λ_I per time unit.

Our proposed methodology generally allows to capture more specific types of blocker mobility. For example, one may decide to relax the assumption of the straight movement and thus model the *walking street* environment, where the user trajectories are not required to remain parallel to the sides of the street. Also note that the straight trajectories of blocker mobility inside the LoS blockage zone are the direct consequence of small dimensions of the said zone, hence resulting in negligible changes of behavior with respect to the angle of motion.

The considered metrics of interest are those pertaining to the temporal behavior of the LoS blockage process and include (i) the mean and the fraction of time in the blocked/non-blocked state as experienced by the Rx, (ii) the residual time in the blocked/non-blocked state, and (iii) the conditional probability that there is blocked/non-blocked state at t_1 given that there was blocked/non-blocked state at t_0 , $t_1 > t_0$.

III. PROPOSED SYSTEM ANALYSIS

All of the three scenarios introduced in the previous Section II can be characterized by following our proposed methodology. The key difference between them is in the distribution of the residence time in the LoS blockage zone (that is, the time that a blocker spends in the LoS blockage zone while crossing it). In this section, we first describe in detail the general method to obtain the distribution of the zone residence time in the LoS blockage for the first scenario (i.e., pedestrian street). For the second and the third scenarios, the corresponding derivations are reported in Appendix A. Finally, we produce the target metrics of interest.

Our step-by-step analytical approach may be summarized as follows:

- Specify the zone, where blockers may occlude the LoS path and thus determine the LoS blockage zone geometry;
- Describe the process of blockage by introducing the alternating renewal process that captures the non-blocked/blocked intervals;
- Obtain the pdf of the non-blocked time interval by analyzing the alternating renewal process in question;
- Produce the pdf of the blocked interval by representing it as a busy period in the $M/GI/\infty$ queuing system, where the service time distribution corresponds to the time spent by a blocker in the LoS blockage zone;
- Calculate all of the metrics of interest, including the moments, the residual time distributions, as well as the conditional non-blocked/blocked states probabilities by applying conventional techniques.

A. LoS Blockage Zone Geometry

Consider the geometrical scenario represented in Fig. 3. Since any blocker entering the zone in question occludes the LoS, the width of the zone equals to the base diameter of

the blocker, d_m . The length of this zone reflects the maximum possible distance, where the height of the blocker still affects the LoS. As illustrated in Fig. 3, from the geometrical considerations the latter follows as

$$r = \frac{r_0(h_B - h_R)}{h_T - h_R} + d_m/2, \quad (1)$$

where r_0 is the distance between the Tx and the Rx, while h_B , h_R , and h_T are the heights of the blocker, the Rx, and the Tx, respectively.

The coordinates of the Tx and the Rx located at the points P and O (see Fig. 3), respectively, are then given by

$$\begin{aligned} x_P &= 0, & y_P &= w_S, \\ x_O &= r_0 \sin(\alpha), & y_O &= w_S - r_0 \cos(\alpha). \end{aligned} \quad (2)$$

The coordinates of the blockage zone vertices are thus

$$\begin{aligned} x_A &= x_O - \frac{d_m}{2} \cos(\alpha), & y_A &= y_O - \frac{d_m}{2} \sin(\alpha), \\ x_B &= x_O + \frac{d_m}{2} \cos(\alpha), & y_B &= y_O + \frac{d_m}{2} \sin(\alpha), \\ x_C &= x_B - r \cos\left(\frac{\pi}{2} - \alpha\right), & y_C &= y_B + r \sin\left(\frac{\pi}{2} - \alpha\right), \\ x_D &= x_A - r \cos\left(\frac{\pi}{2} - \alpha\right), & y_D &= y_A + r \sin\left(\frac{\pi}{2} - \alpha\right), \end{aligned} \quad (3)$$

where α is the angle characterizing the position of the Rx in relation to the Tx location, as shown in Fig. 3.

B. Renewal process analysis

Let ω_j and η_j , $j = 1, 2, \dots$, denote the time spent in the non-blocked and blocked intervals, respectively. As one may observe, these intervals alternate, that is, non-blocked period always precedes the blocked one and vice versa. Since the entry of blockers into the LoS blockage zone is modeled

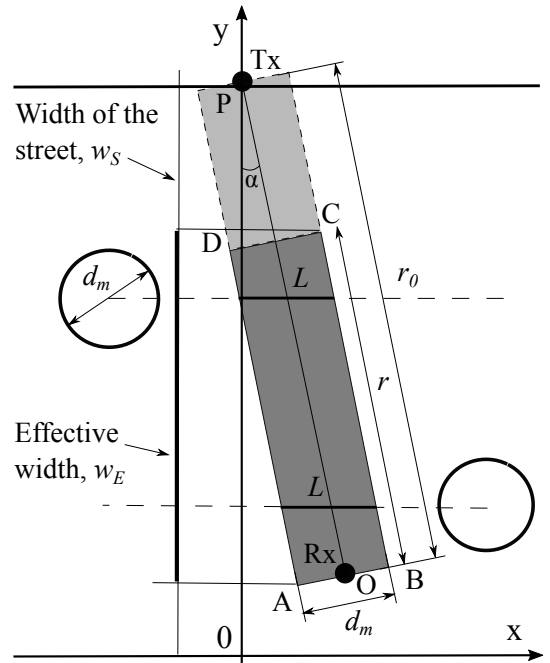


Fig. 3. Geometry of the LoS blockage zone.

$$F_\eta(x) = 1 - \left([1 - F_T(x)] \left[1 - \int_0^x (1 - F_\eta(x-z)) \exp(-\lambda F_T(z)) \lambda dz \right] + \int_0^x (1 - F_\eta(x-z)) |de^{-\lambda F_T(z)}| \right). \quad (4)$$

as a Poisson process, durations of non-blocked and blocked intervals are mutually independent. Hence, the process of the LoS blockage can be modeled as an alternating renewal process, as displayed in Fig. 4. The proposed methodology is valid for all three scenarios.

Define $\xi_j = \omega_j + \eta_j$. The points 0, ξ_1 , $\xi_1 + \xi_2$, and $\xi_1 + \xi_2 + \xi_3$ are the renewal moments that form the process at hand. The density of this process follows from [30] as

$$f(x) = \lambda F_T(x) \exp \left(-\lambda \int_0^x [1 - F_T(y)] dy \right), \quad (5)$$

where λ is the intensity of the blocker arrivals into the zone, $F_T(y)$ is the cumulative distribution function (CDF) of the zone residence time $T = L/V$ for a single blocker, where L is the distance over which one blocker travels inside the blockage zone.

Proposition 1. *The time spent in the non-blocked part, ω_j , follows an exponential distribution with the parameter λ , $F_\omega(x) = 1 - e^{-\lambda x}$, with the mean $\mathbb{E}[\omega] = 1/\lambda$ [31].*

Proof. This result follows directly from the fact that the left-hand sides of the expressions for the time intervals spent in the LoS blockage zone follow a Poisson process in time with the arrival intensity of λ per time unit. Therefore, the time period between the end of an interval, which is considered as an arbitrary point, and the starting point of the next interval is distributed exponentially. \square

Consider now the blocked interval.

Proposition 2. *Let $F_\eta(x)$ be the CDFs of the time in the blocked intervals, η_j , $j = 1, 2, \dots$, with the mean of $\mathbb{E}[\eta]$. The distribution of the blocked interval, $F_\eta(x)$, is the same as the distribution of a busy period in the $M/GI/\infty$ queueing system given by (4), see e.g., [32]. The latter can be evaluated numerically for any $F_T(x)$.*

Proof. Consider the $M/GI/\infty$ queue and associate an indicator function, $I_B(t) = \Pr\{S(t) > 0\}$, where $S(t)$ is the process that describes the number of customers in the system. We observe that a customer arriving when the system is not empty potentially prolongs the busy period. The CDF of the busy period is given in (4). We immediately establish the

analogy with the LoS blockage, where the blockers arriving during the blocked period extend the blockage time. \square

C. Residence Time in the LoS Blockage Zone

To proceed further with deriving the metrics of interest, we require the CDF of the residence time $T = L/V$ in the LoS blockage zone for a single user. Recalling the principles of linear transformation of random variables [33], the probability density function (pdf) of the time $T = L/V$ (for all the three scenarios of interest) reads as

$$f_T(x) = V f_L(xV). \quad (6)$$

Hence, it is sufficient to find the pdf of distance L that one blocker moves inside the LoS blockage zone, f_L , in order to derive f_T . The notation employed in what follows is clarified in Fig. 3. Note that the arrival intensity of the blockers λ that enter the LoS blockage zone is different for all the considered scenarios and is derived in what follows by using λ_I . The latter is the initial arrival intensity of blockers that cross the width of the street for the scenarios one and two (see Fig. 2). For the sake of our analysis, the park/square scenario has the arrival intensity of $\lambda_I = \lambda$.

Note that the derivation of distance L is a scenario-specific part of our analysis as it requires a certain distribution of the entry points of blockers to the LoS blockage zone.

First scenario. Let $F_Y(x)$, $0 \leq x \leq w_S$, be the CDF of the y -coordinate of the entry point for a blocker. As we are only interested in the blockers crossing the blockage area, we truncate this distribution. The resulting truncated distribution $F_{\tilde{Y}}(x)$ is defined on $y_A \leq x \leq y_C$.

The CDF of the distance L traversed by a blocker in the LoS blockage zone is therefore

$$F_L(x) = \begin{cases} 0, & x < 0, \\ F_{\tilde{Y}}(y_C) - F_{\tilde{Y}}(y_C - x \cos(\alpha) \sin(\alpha)) \\ + F_{\tilde{Y}}(y_A) - F_{\tilde{Y}}(y_A - x \cos(\alpha) \sin(\alpha)), & 0 \leq x < x_{min}, \\ 1, & x \geq x_{min}, \end{cases} \quad (7)$$

where $x_{min} = \min(d_m / \cos(\alpha), r / \sin(\alpha))$.

For the pedestrian scenario one (see Fig. 2(a)), (7) takes the form of

$$F_L^1(x) = \begin{cases} 0, & x \leq 0, \\ \frac{x \sin(2\alpha)}{y_C - y_A}, & 0 < x \leq x_{min}, \\ 1, & x > x_{min}. \end{cases} \quad (8)$$

The arrival intensity of the blockers entering the zone that affects the LoS for our first scenario is delivered as

$$\lambda = \lambda_I \frac{w_E}{w_S}, \quad (9)$$

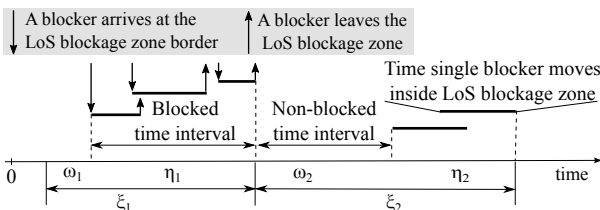


Fig. 4. Renewal process associated with the LoS blockage, where every blocker might spend different time when blocking the LoS.

where w_S is the width of the street, λ_I is the arrival intensity of blockers on the width w_S , and w_E is the effective width, see Fig. 3.

The residence time in the LoS blockage zone for the second and the third scenario is derived in Appendix A.

D. Metrics of Interest

1) *Mean and Fraction of Time in Non-Blocked/Blocked State:* The fraction of time in the non-blocked/blocked state can be produced by utilizing the mean time spent in each state, i.e., [31]

$$\mathbb{E}[T_l] = \frac{\mathbb{E}[\omega]}{\mathbb{E}[\omega] + \mathbb{E}[\eta]}, \quad \mathbb{E}[T_n] = \frac{\mathbb{E}[\eta]}{\mathbb{E}[\omega] + \mathbb{E}[\eta]}, \quad (10)$$

where $\mathbb{E}[\omega]$ and $\mathbb{E}[\eta]$ are the means of the non-blocked/blocked intervals.

Recall that due to the exponential nature of ω , $\mathbb{E}[\omega] = 1/\lambda$. The mean $\mathbb{E}[\eta]$ can be obtained numerically by using (4). However, there is a simpler approach that is outlined below. Observe that the renewal density $f(x)$ is $f(x) = 1/\mathbb{E}[\xi]$, when $t \rightarrow \infty$. From (5), after employing the Laplace transform (LT), we establish that it is also equal to $f(x) = \lambda \exp(-\lambda \mathbb{E}[T])$, where $\mathbb{E}[T]$ is the mean zone residence time for a single blocker, see [18] for details. Hence, we have

$$\mathbb{E}[\xi] = \frac{1}{\lambda} \exp(\lambda \mathbb{E}[T]). \quad (11)$$

Then, $\mathbb{E}[\eta]$ can be established as

$$\begin{aligned} \mathbb{E}[\eta] &= \int_0^\infty [1 - F_\eta(x)] dx \\ &= \int_0^\infty \left(1 - F_\xi(x) - \frac{f_\xi(x)}{\lambda} \right) dx = \mathbb{E}[\xi] - \frac{1}{\lambda}. \end{aligned} \quad (12)$$

Substituting (11) into (12), we arrive at

$$\mathbb{E}[\eta] = \frac{1}{\lambda} [\exp(\lambda \mathbb{E}[T]) - 1]. \quad (13)$$

2) *Residual Time in Non-Blocked/Blocked State:* Here, we characterize the distribution of the residual time spent in the non-blocked/blocked state given that we are currently in the non-blocked/blocked state. Recall that the distribution of the non-blocked interval is exponential, while the CDF for the blocked interval is provided in (4). Hence, the residual time distribution in the non-blocked state is also exponential with the same parameter. Therefore, the residual blocked time CDF is

$$F_{t_\eta}(t) = \frac{1}{\mathbb{E}[\eta]} \int_0^t [1 - F_\eta(y)] dy, \quad (14)$$

and the residual non-blocked time CDF is

$$F_{t_\omega}(t) = 1 - e^{-\lambda t}, \quad t \geq 0. \quad (15)$$

3) *Conditional Non-Blocked/Blocked State Probabilities:* Consider now two instants of time, $t_0 = 0$ and t_1 , $t_1 - t_0 = t > 0$. Denoting the non-blocked and the blocked states by 0 and 1, respectively, we are interested in calculating the conditional probabilities, $p_{00}(t)$, $p_{01}(t)$ as well as $p_{10}(t)$, $p_{11}(t)$ that there is non-blocked/blocked state at t_1 given that there was non-blocked/blocked state at t_0 . The general solution for this problem follows from [31] and particularly $p_{00}(t)$ can be established as

$$p_{00}(t) = \frac{\mathbb{E}[\omega]}{\mathbb{E}[\omega] + \mathbb{E}[\eta]} + \frac{g(t)}{\mathbb{E}[\omega]}, \quad (16)$$

where $g(t)$ has the LT of

$$g^*(s) = \frac{\mathbb{E}[\omega]\mathbb{E}[\eta]}{(\mathbb{E}[\omega] + \mathbb{E}[\eta])s} - \frac{(1 - f_\omega^*(s))(1 - f_\eta^*(s))}{s^2(1 - f_\omega^*(s)f_\eta^*(s))}, \quad (17)$$

where $f_\omega^*(s)$ and $f_\eta^*(s)$ are the LTs of $f_\omega(x)$ and $f_\eta(x)$, respectively.

In our target case, the density of the blocked period is not available in a closed form, thus preventing from transitioning to the LT domain. For practical calculations, we propose a simpler approach by utilizing the time domain convolutions as discussed below. Observe that the probabilities $p_{00}(\Delta t)$ and $p_{01}(\Delta t)$ can be represented as

$$\begin{aligned} p_{00}(\Delta t) &= \sum_{i=0}^{\infty} \mathbb{P}\{A_i(\Delta t)\}, \\ p_{01}(\Delta t) &= \sum_{i=1}^{\infty} \mathbb{P}\{B_i(\Delta t)\}, \end{aligned} \quad (18)$$

where $A_i(t)$ are the events corresponding to starting in the non-blocked interval at t_0 and ending in the non-blocked interval after some $\Delta t = t_1 - t_0$, while having exactly i , $i = 0, 1, \dots$, blocked periods during Δt . Similarly, $B_i(t)$ are the events corresponding to starting in the non-blocked interval at t_0 and ending in the blocked interval at t_1 , while having exactly i , $i = 1, 2, \dots$, non-blocked periods during Δt .

The probability of the event A_0 , which is defined as residing in the non-blocked interval ω at time t_1 given that the system was in the same non-blocked state ω at time t_0 , is produced by

$$\mathbb{P}\{A_0(\Delta t)\} = 1 - F_{t_\omega}(\Delta t), \quad (19)$$

where $F_{t_\omega}(\Delta t)$ is the residual time in the non-blocked period as obtained in (15).

The probability of the event B_1 , which is defined as residing in the blocked interval η at time t_1 given that the system was in the preceding non-blocked state ω at time t_0 , is

$$\begin{aligned} \mathbb{P}\{B_1(\Delta t)\} &= 1 - (F_\eta * F_{t_\omega})(\Delta t) - (1 - F_{t_\omega}(\Delta t)) \\ &= F_{t_\omega}(\Delta t) - (F_\eta * F_{t_\omega})(\Delta t), \end{aligned} \quad (20)$$

where F_η is the CDF of the blocked interval from (4) and $*$ denotes the convolution operation.

Further, consider the event A_1 corresponding to when the Rx is in the non-blocked interval at time t_1 given that it was in the preceding non-blocked interval at time t_0 (there

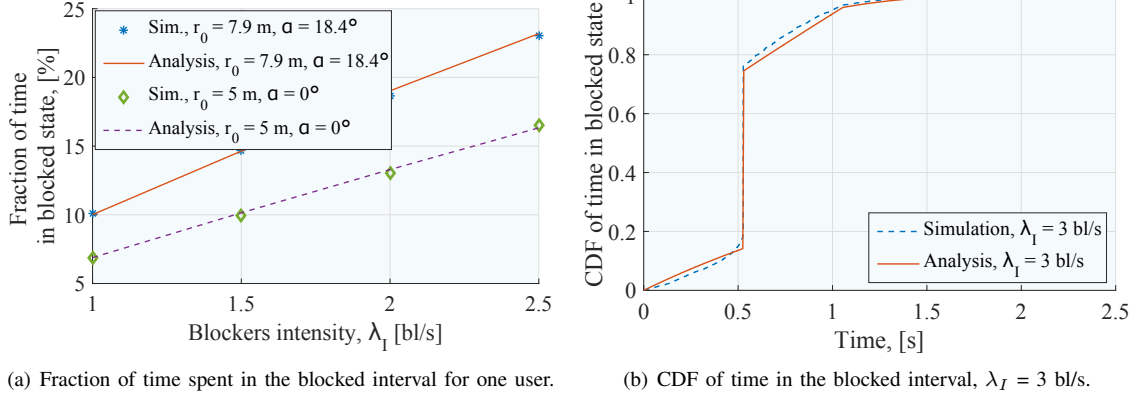


Fig. 5. Benchmarking the analytical model against the simulation results for the first usage scenario.

is a blocked interval embedded in between t_0 and t_1). The probability of this event is

$$\mathbb{P}\{A_1(\Delta t)\} = (F_\eta * F_{t_\omega})(\Delta t) - (F_\omega * F_\eta * F_{t_\omega})(\Delta t), \quad (21)$$

where F_ω is the CDF of the non-blocked interval.

Finally, the probability of the event B_2 that the Rx is in the blocked interval at t_1 given that it was in the preceding blocked interval at t_0 (there is a non-blocked interval embedded in between t_0 and t_1), is established as

$$\begin{aligned} \mathbb{P}\{B_2(\Delta t)\} &= (F_\omega * F_\eta * F_{t_\omega})(\Delta t) \\ &\quad - (F_\eta * F_\omega * F_\eta * F_{t_\omega})(\Delta t). \end{aligned} \quad (22)$$

The probabilities $p_{10}(\Delta t)$ and $p_{11}(\Delta t)$ may be obtained similarly.

IV. ACCURACY ASSESSMENT AND NUMERICAL ANALYSIS

In this section, we first assess the accuracy of our proposed model with a benchmarking against system-level simulations. Then, we proceed by characterizing the extent of temporal dependence under study as a function of the input parameters.

A. Accuracy Assessment

We first benchmark the constructed analytical model by utilizing our in-house simulation framework developed specifically for the purposes of this study. For the sake of exposition, we assume that the location of the user device of interest is fixed. The initial number of deployed blockers is calculated based on the arrival intensity of blockers entering the cell, λ_I . Particularly, considering the first usage scenario, whenever the simulation is started, new blockers appear at the cell edge of length w_S according to a Poisson process with the arrival intensity of λ_I . Blockers then move around across the deployment with the constant speed up to the edge of the deployment area.

Fig. 5(a) reports on the average user blockage time obtained by using simulations as well as produced with the proposed analytical model. As one may observe, the analytical results agree well with the simulation data, while both increase linearly with the growing arrival intensity of blockers. To assess the time correlation in the non-blocked/blocked state, the CDF of blocked duration is displayed in Fig. 5(b). Here,

TABLE II
BASELINE SYSTEM PARAMETERS

Parameter	Value
Height of Tx, h_T	3 m
Height of Rx, h_R	1.3 m
Height of a blocker, h_B	1.7 m
Diameter of a blocker, d_m	0.5 m
Speed of a blocker, V	1 m/s
Width of the street, w_S	5 m
Angle, α	$\pi/6$
Frequency	28 GHz
Bandwidth, B	1 GHz
Noise level	-114 dB
Transmit power	0 dB

close match between the analytical and the simulation results is also clearly visible. Small mismatch between simulation and analysis is caused by the specifics of our analytical model. Particularly, in simulations we explicitly model the LoS blockage zone by taking into account the circular nature of the user. In the developed mathematical model, the LoS blockage zone is assumed to be of rectangular shape thus neglecting the curvature caused by the user, see Section III for details. Although one could extend the model to the case of more complex geometry of the LoS blockage zone leading to more complex expressions, the resulting error of approximation by a rectangle is negligible.

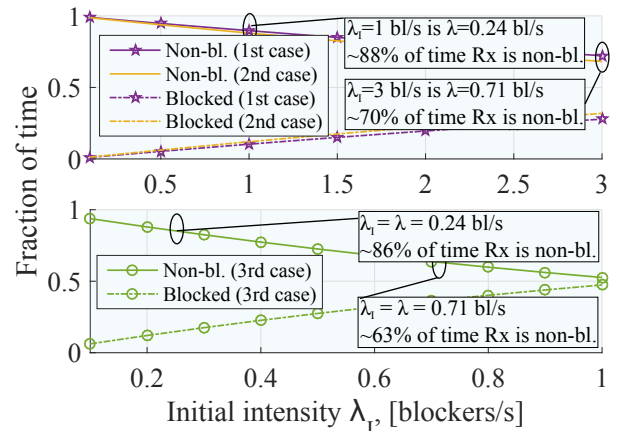


Fig. 6. Fraction of time in non-blocked/blocked state as a function of λ_I .

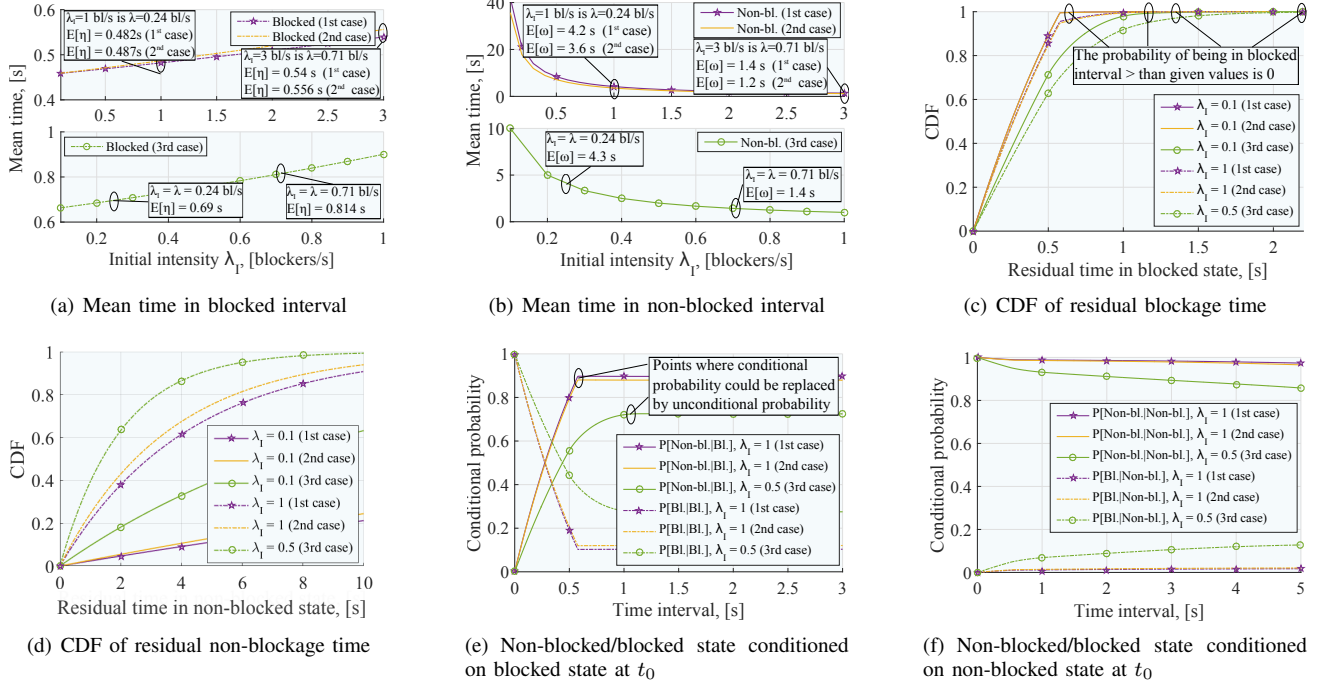


Fig. 7. Mean and residual time in non-blocked/blocked state and conditional probability of non-blocked/blocked state given that Rx is non-blocked/blocked.

B. Numerical Analysis

We now proceed with analyzing the response of the blockage-related metrics to the selected ranges of input mmWave system parameters. We thus consider the key performance indicators in the deployment of interest, namely, the fraction of time spent in the non-blocked/blocked state as illustrated in Fig. 6. It is a function of the arrival intensity of blockers, λ_I , for all the three scenarios under study. The parameters for the two scenarios that are collected in the plot are shown in Table II.

For the purposes of a numerical comparison, consider the initial intensities for the first and the second scenario to be equal to 1 and 3 blockers per second, respectively. This corresponds to the following intensities of entering the LoS zone: 0.24 and 0.71 blockers per second. The initial arrival intensity is equal to the intensity of entering the LoS zone for the third scenario. Clearly, as the arrival intensity of blockers grows, the fraction of time spent in the non-blocked/blocked state decreases/increases correspondingly. The main observation here is that the resulting trend is close to linear. One may notice further that for the arrival intensity of 0.24 blockers per second the fraction of time spent in the non-blocked/blocked state is almost the same for all the three scenarios. As the arrival intensity increases and approaches the value of 0.71, the difference between the first two scenarios and the third case becomes more considerable.

Fig. 7(a) and 7(b) report on the absolute values of the mean time spent in the non-blocked/blocked state for the same input parameters. As one may observe, the mean time spent in the non-blocked state decreases significantly as λ_I increases from 0 to 3. However, the difference between the three scenarios for two selected intensities is not significant. The mean time spent in the blocked state is the longest for the third scenario. It may

be explained by the fact that the possible walking distance of a blocker is higher in this third scenario, since the blocker can move closer to the diagonal inside the rectangle. Note that the blocked state behavior does not change drastically over a wide range of the considered blocker intensities. This is because even for higher intensities of blockers the blocked intervals are likely to feature only a single blocker occluding the LoS.

The mean time spent in the non-blocked/blocked state together with the associated fractions produce a direct implication on the dimensioning of mmWave systems. More specifically, using an appropriate propagation model, such as the one presented in [4], as well as accounting for the set of the modulation and coding schemes, one can evaluate the average throughput of a user located at a certain distance from the mmWave AP over a particular time slot. Given a certain value of the target mean data rate at the input, this information can be used further for determining the optimal coverage of a single mmWave AP.

In Fig. 7(c) and 7(d), the CDFs of residual time in the blocked/non-blocked state are shown. As one may observe, the probability for the time spent in the blocked interval to exceed the blocker mean residence time is rather small. For example, the mean time in blocked interval for the 1st case with $\lambda_I = 1$ bl/s is approximately 0.5 s and the CDF $F_{t_\eta}(t < 0.5) = 0.9$ roughly. This fact implies that for a wide range of the considered intensities, in most cases, the blocked interval coincides with the residence time of a single blocker. Therefore, a user enters the non-blocked state after a certain time interval, which mainly depends on the size and the speed of the blocker, and less so on the arrival intensity of the blockers (note that the mean time in the blocked interval, Fig. 7(a), and the CDF of residual time in the blocked state, Fig. 7(c), do not change drastically with increasing arrival

intensity of blockers). Generally, knowing that the Rx is in the blocked interval, one can estimate the remaining time in this period. This may reduce the amounts of signaling information required for tracking the state of mmWave receivers. Also, the shape of the CDF curves for the residual time in the blocked interval is explained by the particular behavior of the CDF of time for a single blocker movement inside the LoS blockage zone, which has a distinct plateau.

Fig. 7(e) and 7(f) illustrate the behavior of the conditional probability to be in the non-blocked/blocked state at time t_1 given that the Rx was in the non-blocked/blocked state at time $t_0 = 0$, $t_1 > t_0$. Due to the long average time in the non-blocked state as compared to the average time in the blocked state, the probability to change the state from non-blocked to blocked is rather small for the considered values of t_1 . In contrast, the probability to become non-blocked given that the Rx was blocked at time t_0 increases significantly. After that, the conditional probability converges to the unconditional one and the process in question “loses” its memory.

V. SELECTED APPLICATIONS OF OUR METHODOLOGY

This section first summarizes two important analytical results stemming from the direct application of our proposed methodology. Then, we continue by demonstrating the achievable performance gains in terms of the computation complexity after applying our model in system-level evaluation of mmWave systems.

A. Optimal Height of the mmWave AP

Let us first determine the height of the mmWave AP, such that the average path loss to the user is minimal. To this end, we utilize our blocker mobility model to estimate the fraction of time in the non-blocked state as a function of h_T , and then apply the mmWave propagation model from [4] to characterize the mean path loss as a function of h_T .

The average path loss can thus be established as in [18]

$$L_e = \mathbb{E}[T_l]L_{LoS} + (1 - \mathbb{E}[T_l])L_{nLoS}, \quad (23)$$

where $\mathbb{E}[T_l]$ is the fraction of time that the Rx spends in the non-blocked state, which has been derived in (14), while L_{LoS} and L_{nLoS} are the path loss values for the LoS and the nLoS components as obtained in [4].

For any value of the arrival intensity of blockers, the optimal height of the mmWave AP can now be established by utilizing the graphical approach and plotting (23) to identify the value minimizing the average path loss. To vary the arrival intensity of blockers that enter the LoS blockage zone proportionally to its dimensions, we assume that $\lambda_S = 0.1$ bl/s is the arrival intensity of blockers crossing the unit square area. The intensity of blockers entering the LoS blockage zone can then be written as $\lambda = \lambda_S r d_m$.

Fig. 8(a) demonstrates the optimal Tx height for different cell radius values in the square scenario (the third case). Here, the constant arrival intensity of blockers is set to $\lambda_S = 0.1$ bl/s, while the remaining parameters are given in Table II. As one may learn, an increase in the cell radius requires the mmWave Tx to be deployed higher in order to achieve the

optimized propagation conditions. Further, Fig. 8(b) illustrates the optimal height of the Tx for a fixed cell radius of 30 m and different intensities of blockers that enter the unit square area of LoS blockage zone, λ_S . It could be noticed that with the growing blocker arrival intensity the optimal height of the mmWave Tx increases as well. This effect is explained by the fact that the probability of residing in the non-blocked state decreases; hence, one needs to increase the height of the Tx to maximize the fraction of time spent in the non-blocked state.

B. Cell Range Analysis

Another direct application of our proposed model is to determine the maximum coverage range of the mmWave AP, such that a certain average data rate is delivered to all of the users. The latter can be achieved by ensuring that the user data rate at the cell edge is higher than the required minimum.

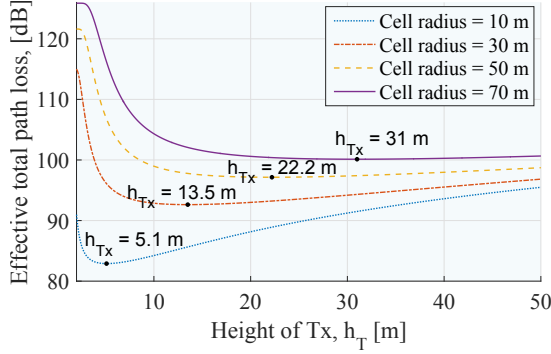
Assume a Poisson field of users in \mathbb{R}^2 with the density of λ_N users per square unit. Let x be the intended radius of the mmWave coverage zone. The number of users in this covered area follows a Poisson distribution with the parameter $\lambda_N \pi x^2$. The traffic model is considered here to be “full buffer”, that is, the mmWave system is observed in the highly-loaded conditions. We are interested in determining the maximum radius x , such that the capacity of at least k Mbps is provided to each user. The bandwidth of the mmWave system, B , is allowed to be infinitesimally divisible. For simplicity, we consider an equal division of bandwidth between all of the users, even though any reasonable resource allocation mechanism can in principle be assumed, e.g., max-min or proportional fair [34].

The capacity delivered to the mmWave Rx located at x can be derived as

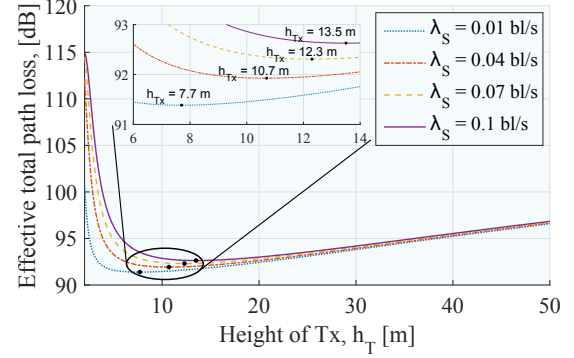
$$R(x) = cB_i \log[1 + S(x)], \quad (24)$$

where B_i is the bandwidth made available to the user of interest, $S(x)$ is the average signal-to-noise ratio (SNR) at this user, and c is a constant accounting for imperfections of the modulation and coding schemes. In what follows, we set $c = 1$ for simplicity.

Since the radio resource in the system is assumed to be equally distributed between all of the users, the bandwidth share actually available to the Rx located at x is $B_i = B/N$, where N is a discrete random variable (RV) having a Poisson distribution with the density of $\lambda_N \pi x^2$ per considered area of interest. To obtain the SNR $S(x)$, we employ the measurement-based mmWave propagation model in [4] by defining as $s_0(x)$ the SNR associated with the LoS state and as $s_1(x)$ the SNR associated with the nLoS state. The aggregate SNR is a two-valued discrete RV taking the values of $s_i(x)$, $i = 0, 1$, with the probabilities corresponding to the fraction of time spent in the non-blocked ($\mathbb{E}[T_l]$) and blocked ($1 - \mathbb{E}[T_l]$) state, respectively. The RVs B_i and $S(x)$ are independent and their joint probability mass function (pmf) is derived as the product of the individual pmfs. Once this joint pmf is obtained,

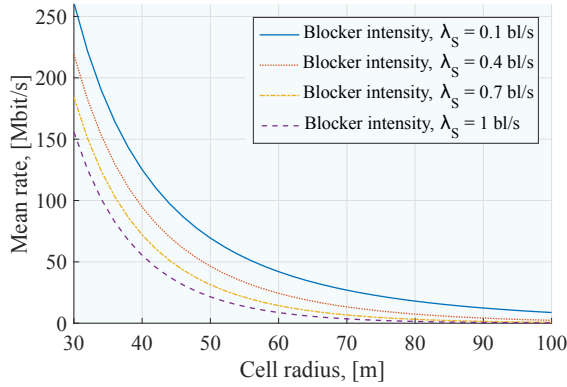


(a) Varying the cell radius

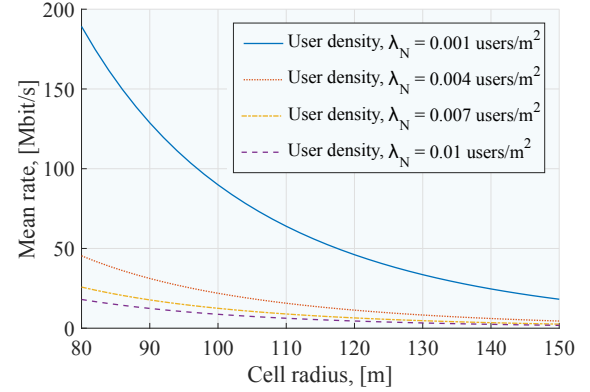


(b) Varying the arrival intensity of blockers

Fig. 8. Optimal height of the mmWave AP vs. cell radius and arrival intensity of blockers.



(a) Varying the cell radius and blocker arrival intensity



(b) Varying the cell radius and user density

Fig. 9. Mean rate at the cell edge vs. cell radius, user densities, and blocker arrival intensities.

we may proceed with determining the mean capacity $R(x_c)$ that is provided to a user located at the cell edge x_c as

$$\begin{aligned} \mathbb{E}[R] = & \sum_{N=1}^{\infty} \frac{(\lambda_N \pi x_c^2)^N (e^{-\lambda_N \pi x_c^2})}{N!} \times \\ & \times \left(\mathbb{E}[T_l] c \frac{B}{N} \log[1 + s_0(x_c)] + \right. \\ & \left. + (1 - \mathbb{E}[T_l]) c \frac{B}{N} \log[1 + s_1(x_c)] \right), \end{aligned} \quad (25)$$

which can be evaluated numerically.

The mean capacity made available to a user located at the cell edge x_c , for different user and blocker intensities, is

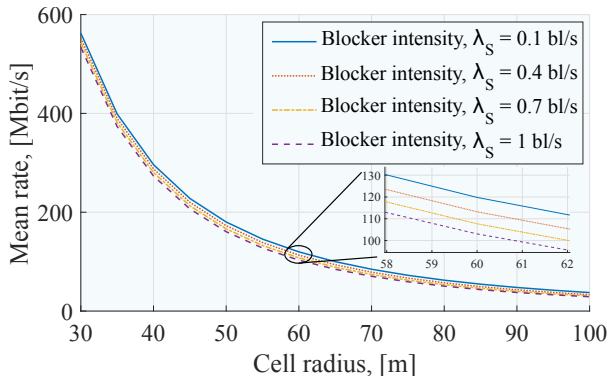


Fig. 10. Mean rate vs. cell radius, user, and blocker arrival intensities.

reported in Fig. 9. It is a function of the cell radius as well as the user and blocker intensities. The rest of the parameters are collected in Table II. In Fig. 9(a), the density of the users is set as $\lambda_N = 0.01$ users/m², and the height of the mmWave Tx is assumed to be $h_T = 10$ m. As an example, these plots correspond to our third scenario of interest. As one may observe, the mean data rate decreases as the cell range and/or the arrival intensity of blockers grows. In addition, the cell radius delivering a certain target mean data rate shrinks as the density of users increases. Provided with a particular target data rate, one may use Fig. 9 to estimate the maximum cell radius for given blocker and user intensities, such that the chosen data rate is made available to all of the mmWave users.

In addition to the above, the analytical formulation for the mean rate $R(x)$ of each user in the cell is given as

$$\begin{aligned} \mathbb{E}[R] = & \sum_{N=1}^{\infty} \frac{(\lambda_N \pi x^2)^N (e^{-\lambda_N \pi x^2})}{N!} c \frac{B}{N} \times \\ & \times \int_0^{x_c} \left(\mathbb{E}[T_l(x)] \log[1 + s_0(x)] + \right. \\ & \left. + (1 - \mathbb{E}[T_l(x)]) \log[1 + s_1(x)] \right) f_{X_U}(x) dx, \end{aligned} \quad (26)$$

where $f_{X_U}(x) = 2x/x_c^2$ is the pdf of the distance X_U between Tx and Rx uniformly distributed in the cell of the radius x_c , while the fraction of time in non-blocked state is obtained by

TABLE III
ABSOLUTE RUN TIME MEASUREMENTS IN SLS EVALUATION, S.

λ_I , bl./s.		0.1	0.3	0.5	0.7	1.0
T_U , ms						
100	simulation	0.101	0.215	0.532	0.860	0.928
	analysis	0.250	0.272	0.243	0.256	0.292
70	simulation	0.208	0.290	0.820	1.356	2.801
	analysis	0.342	0.398	0.287	0.316	0.351
50	simulation	0.581	1.012	1.91	3.282	5.982
	analysis	0.681	0.538	0.369	0.694	0.499
10	simulation	1.211	3.921	5.867	7.119	10.92
	analysis	2.968	3.690	1.762	2.774	2.104
1	simulation	10.28	21.40	54.91	78.92	1.24e2
	analysis	22.64	18.18	23.98	19.09	22.11

using (10) and (13) as

$$\mathbb{E}[T_l(x)] = \frac{1}{\exp(\lambda \mathbb{E}[T])}, \quad (27)$$

where $\mathbb{E}[T]$ is the mean residence time.

The mean rate of a randomly selected user in the cell is illustrated in Fig. 10. As one may observe, increasing the arrival intensity of blockers entering unit area of the LoS blockage zone, λ_S , does not drastically affect the mean rate of a randomly selected user, as opposed to the mean rate at the cell edge.

C. System-Level Simulation Complexity

Today, the performance of complex wireless systems is primarily assessed within large-scale system-level simulation (SLS, see e.g., [35]) environments. Our proposed mathematical model can be efficiently utilized as part of an SLS tool to substitute for the need to explicitly model the blockage process. This may drastically improve the simulation run times, especially in highly crowded urban scenarios.

In Table III, we report on the computation complexity measurements in terms of the SLS run time as a function of the blocker arrival intensity and the *environment update interval*, T_U for the two cases: (i) direct simulation of the blockage process and (ii) application of our proposed model. From the SLS perspective, the environment update interval corresponds to how frequently we monitor the state of the users. In the latter case, each user has been associated with the pdf of the non-blocked and blocked intervals, thus implying that we only need to update its state whenever the said interval expires. In the former direct modeling approach, at each environment update interval, we have to re-estimate the state of the users by employing the straightforward geometry considerations. Doing so significantly increases the computation complexity of the SLS evaluation, especially in dense environments. Our experiments were conducted for the following parameters: the distance between the mmWave AP and the user is $r_0 = 10$ m and the blocker speed is $V = 1$ m/s. The simulation time was set to 50 s, while the hardware parameters were Intel Core i7-6700HQ CPU, 2.60 GHz (1 core run), and 32 GB RAM.

As it can be established by analyzing Table III, the complexity of both simulation and analysis grows as the environment update interval decreases. Even though the simulation run time does not depend on the blocker density (nor on the distance

between the mmWave AP and the Rx), the SLS modeling complexity increases with a higher number of blockers. This is because the computation complexity is associated with the need to characterize an intersection with every blocker to determine the current state of each user. For the SLS results reported in this work, we deploy blockers at the edge of the modeled scenario and mimic their movement across the street. From the simulation perspective, computation complexity grows linearly as blocker arrival intensity increases, i.e., the overall modeling complexity is $O(n)$. Although the use of sophisticated techniques, such as spatial hashing, may reduce the complexity down to $O(\log(n))$ at the expense of more cumbersome implementation, the resulting complexity would still grow rapidly for higher user densities. In stark contrast, with our proposed analytical modeling, the complexity remains constant at $O(1)$. Finally, with decreasing update interval T_U , both analytical and simulation complexity grow linearly ($O(n)$). However, it may be not as important, because the value of $T_U < 1$ ms is seldom used in practical systems.

VI. CONCLUSIONS

In this paper, we systematically characterized the effects of the LoS blockage in cellular mmWave systems with mobile blockers. The mathematical process in question was shown to be of alternating renewal nature, where the non-blocked periods interchange with the blocked intervals. The distribution of the non-blocked intervals was shown to have a simple memoryless exponential form, while the blocked periods were established to follow a general distribution. Three characteristic urban scenarios – as discussed in the corresponding 3GPP specifications – were considered as examples. Our resulting model allowed for establishing the performance metrics of interest, including the mean and the fraction of time spent in the non-blocked/blocked state as well as the time-dependent conditional probabilities for the latter. In addition, we discussed several important practical applications of our proposed methodology, including optimization of the mmWave AP height, mmWave cell range analysis, and system-level modeling complexity reduction.

Relying on the developed mathematical methodology, we then analyzed the effects of the LoS blockage by demonstrating that there exists a strong temporal correlation for the timescales of interest in mmWave systems (i.e., less than about a second). We believe that our contributed temporal statistics could be useful for modeling human body blockage in the mmWave system simulation tools as well as in designing mmWave communication functions.

ACKNOWLEDGMENT

This work is supported by Intel Corporation and the Academy of Finland.

APPENDIX A

RESIDENCE TIME IN THE LOS BLOCKAGE ZONE

Here, we derive the CDFs of the residence time in the LoS blockage zone for the pathway and the park/square/stadium scenarios (see Fig. 2).

Second scenario. Consider the pathway scenario. Here, the main difference as compared to the pedestrian scenario is in that the users tend to move closer to the central lane of the street. We model this effect by using the triangular distribution with the following CDF

$$F_Y(x) = \begin{cases} 0, & x \leq 0, \\ \frac{x^2}{w_S c}, & 0 < x \leq c, \\ 1 - \frac{(w_S - x)^2}{w_S(w_S - c)}, & c < x \leq w_S, \\ 1, & x > w_S, \end{cases} \quad (28)$$

where c is the mode.

The distribution of distance, which is traveled by a blocker in the blockage zone, depends on the position of the LoS blockage zone with respect to the mode of the triangular distribution. We have the following five different cases:

1) If $y_C \leq c$:

$$F_L^{2,1}(x) = \begin{cases} 0, & x \leq 0, \\ \frac{x \sin(2\alpha)}{y_C - y_A}, & 0 < x \leq x_{\min}, \\ 1, & x > x_{\min}. \end{cases} \quad (29)$$

2) If $y_C - y_{\min} \leq c < y_C$, $y_{\min} = x_{\min} \cos(\alpha) \sin(\alpha)$:

$$F_L^{2,2}(x) = \begin{cases} 0, & x \leq 0, \\ \frac{\sin(2\alpha)(4c(y_A + y_C) - w_S(x \sin(2\alpha) + 4(c + y_A)))}{4w_S(y_A^2 + c(c - 2y_C)) + c(y_C^2 - y_A^2)}, & 0 \leq x < \frac{y_C - c}{\sin(\alpha) \cos(\alpha)}, \\ \frac{w_S(c - y_C)^2 + x \sin(2\alpha)(c - w_S)(y_A + y_C)}{w_S(y_A^2 + c(c - 2y_C)) + c(y_C^2 - y_A^2)}, & \frac{y_C - c}{\sin(\alpha) \cos(\alpha)} < x \leq x_{\min}, \\ 1, & x > x_{\min}. \end{cases}$$

3) If $y_A + y_{\min} \leq c < y_C - y_{\min}$:

$$F_L^{2,3}(x) = \begin{cases} 0, & x \leq 0, \\ \frac{x \sin(2\alpha)(4c(y_A + y_C) - w_S(x \sin(2\alpha) + 4(c + y_A)))}{4(w_S(y_A^2 + c(c - 2y_C)) + c(y_C^2 - y_A^2))}, & 0 < x \leq x_{\min}, \\ 1, & x > x_{\min}. \end{cases} \quad (31)$$

4) If $y_A \leq c < y_A + y_{\min}$:

$$F_L^{2,4}(x) = \begin{cases} 0, & x \leq 0, \\ \frac{x \sin(2\alpha)(4c(y_A + y_C) - w_S(x \sin(2\alpha) + 4(c + y_A)))}{4(w_S(y_A^2 + c(c - 2y_C)) + c(y_C^2 - y_A^2))}, & 0 < x \leq \frac{c - y_A}{\sin(\alpha) \cos(\alpha)}, \\ \frac{w_S(c - y_A)^2 + x \sin(2\alpha)(y_A + y_C - 2w_S)}{w_S(y_A^2 + c(c - 2y_C)) + c(y_C^2 - y_A^2)}, & \frac{c - y_A}{\sin(\alpha) \cos(\alpha)} < x \leq x_{\min}, \\ 1, & x > x_{\min}. \end{cases} \quad (32)$$

5) If $c \leq y_A$:

$$F_L^{2,5}(x) = \begin{cases} 0, & x \leq 0, \\ \frac{x \sin(2\alpha)}{y_C - y_A}, & 0 < x \leq x_{\min}, \\ 1, & x > x_{\min}. \end{cases} \quad (33)$$

The arrival intensity of the blockers that enter the zone, which affects the LoS for the second scenario is given as follows

$$\lambda = \lambda_I (F_Y(y_C) - F_Y(y_A)). \quad (34)$$

The above may be explained by the fact that the majority of blockers cross the width of the street in the middle by following the triangular distribution for the entry point. Therefore, the Poisson process in time has the arrival intensity of emerging at the effective width per time unit, w_E , equal to λ as derived in (34).

Third scenario. Finally, for the park/stadium/square scenario, the CDF of distance that is walked by a blocker in the blockage zone is a mixture of distributions in the following form

$$F_L^3(x) = \begin{cases} 0, & x \leq 0, \\ w_1 F_L^{3,1}(x) + w_2 F_L^{3,2}(x), & 0 < x \leq \sqrt{d_m^2 + r^2}, \\ 1, & x > \sqrt{d_m^2 + r^2}, \end{cases} \quad (35)$$

where the weights are given by

$$w_1 = \frac{d_m^2 + 3d_m r}{d_m^2 + 3d_m r + 2r^2}, \quad w_2 = \frac{2r^2}{d_m^2 + 3d_m r + 2r^2}, \quad (36)$$

and the corresponding CDFs are

$$F_L^{3,1}(x) = \begin{cases} 0, & x \leq 0, \\ \frac{\pi x^2}{4r d_m}, & 0 < x \leq \min(r, d_m), \\ \frac{1}{2r d_m} (\min(r, d_m) \sqrt{x^2 - \min(r, d_m)^2} + x^2 \arcsin(\frac{\min(r, d_m)}{x})), & \min(r, d_m) < x \leq \max(r, d_m), \\ \frac{1}{2r d_m} (\min(r, d_m) \sqrt{\max(r, d_m)^2 - \min(r, d_m)^2} + d_m (\sqrt{x^2 - d_m^2} - \sqrt{\max(r, d_m)^2 - d_m^2}) + r (\sqrt{x^2 - r^2} - \sqrt{\max(r, d_m)^2 - r^2}) + \max(r, d_m)^2 (\arccos(\frac{r}{\max(r, d_m)}) + \arcsin(\frac{\min(r, d_m)}{\max(r, d_m)}) - \arcsin(\frac{d_m}{\max(r, d_m)})) + x^2 (\arcsin(\frac{d_m}{x}) - \arccos(\frac{r}{x}))), & \max(r, d_m) < x \leq \sqrt{d_m^2 + r^2}, \\ 1, & x > \sqrt{d_m^2 + r^2}, \end{cases}$$

$$F_L^{3,2}(x) = \begin{cases} 0, & x \leq d_m, \\ \frac{d_m^2 - x^2 + 2r \sqrt{x^2 - d_m^2}}{r^2}, & d_m < x \leq \sqrt{d_m^2 + r^2}, \\ 1, & x > \sqrt{d_m^2 + r^2}. \end{cases} \quad (37)$$

The arrival intensity of the blockers that enter the zone, which affects the LoS for the third scenario is then $\lambda = \lambda_I$.

REFERENCES

- [1] J. G. Andrews, S. Buzzi, C. Wan, S. V. Hanly, A. Lozano, A. C. K. Soong, and J. C. Zhang, "What will 5G be?," *IEEE Journal on Selected Areas in Communications*, vol. 32, pp. 1065–1082, June 2014.
- [2] A. Ghosh, T. A. Thomas, M. C. Cudak, R. Ratasuk, P. Moorut, F. W. Vook, T. S. Rappaport, G. R. MacCartney, S. Sun, and S. Nie, "Millimeter-wave enhanced local area systems: a high-data-rate approach for future wireless networks," *IEEE Journal on Selected Areas in Communications*, vol. 32, pp. 1152–1163, June 2014.

- [3] T. S. Rappaport, S. Sun, R. Mayzus, H. Zhao, Y. Azar, K. Wang, G. N. Wong, J. K. Schulz, M. K. Samimi, and F. Gutierrez Jr., "Millimeter wave mobile communications for 5G cellular: It will work!," *IEEE Access*, vol. 1, pp. 335–349, May 2013.
- [4] M. R. Akdeniz, Y. Liu, M. K. Samimi, S. Sun, S. Rangan, T. S. Rappaport, and E. Erkip, "Millimeter wave channel modeling and cellular capacity evaluation," *IEEE Journal on Selected Areas in Communications*, vol. 32, pp. 1164–1179, June 2014.
- [5] C. Gustafson, F. Tufvesson, K. Wyne, S. Haneda, and A. F. Molisch, "Directional analysis of measured 60 GHz indoor radio channels using SAGE," in *IEEE Vehicular Technology Conference (VTC Spring)*, May 2011.
- [6] 3GPP, "Further advancements for E-UTRA physical layer aspects (Release 9)," 3GPP TR 36.814 V9.0.0, 2010.
- [7] METIS, "Initial channel models based on measurements," METIS deliverable D1.2, April 2014.
- [8] 3GPP, "Channel model for frequency spectrum above 6 GHz (Release 14)," 3GPP TR 38.900 V2.0.0, 2016.
- [9] COST IC1004, "Channel measurements and modeling for 5G networks in the frequency bands above 6 GHz," white paper, April 2016.
- [10] S. Hur, S. Baek, B. Kim, Y. Chang, A. F. Molisch, T. S. Rappaport, K. Haneda, and P. J., "Proposal on millimeter-wave channel modeling for 5G cellular system," *IEEE Journal on Selected Areas in Communications*, vol. 10, pp. 454 – 469, April 2016.
- [11] S. Sun, T. Rappaport, T. A. Thomas, H. C. A. Ghosh, Nguyen, I. Z. Kovacs, I. Rodriguez, O. Koymen, and A. Partyka, "Investigation of prediction accuracy, sensitivity, and parameter stability of large-scale propagation path loss models for 5G wireless communications," *IEEE Transactions on Vehicular Technology*, vol. 65, pp. 2843–2860, May 2016.
- [12] M. Zhang, M. Mezzavilla, R. Ford, S. Rangan, S. S. Panwar, E. Mellios, D. Kong, A. R. Nix, and M. Zorzi, "Transport layer performance in 5G mmWave cellular," in *IEEE Conference on Computer Communications Workshops (INFOCOM WKSHPS)*, Available: <http://arxiv.org/abs/1603.02701>, 2016.
- [13] M. Mezzavilla, S. Dutta, M. Zhang, M. R. Akdeniz, and S. Rangan, "5G mmwave module for the ns-3 network simulator," in *ACM International Conference on Modeling, Analysis and Simulation of Wireless and Mobile Systems*, 2015.
- [14] K. Haneda *et al.*, "5G 3GPP-like channel models for outdoor urban microcellular and macrocellular environments," in *IEEE Vehicular Technology Conference (VTC 2016-Spring)*, May 2016.
- [15] T. Bai, R. Vaze, and R. W. Heath Jr., "Using random shape theory to model blockage in random cellular networks," in *International Conference on Signal Processing and Communications (SPCOM)*, July 2012.
- [16] T. Bai, R. Vaze, and R. W. Heath Jr., "Analysis of blockage effects on urban cellular networks," *IEEE Transactions on Wireless Communications*, vol. 13, pp. 5070–5083, September 2014.
- [17] M. Abouelseoud and G. Charlton, "The effect of human blockage on the performance of millimeter-wave access link for outdoor coverage," in *IEEE Vehicular Technology Conference (VTC Spring)*, June 2013.
- [18] M. Gapeyenko, A. Samuylov, M. Gerasimenko, D. Moltchanov, S. Singh, E. Aryafar, S. Yeh, N. Himayat, S. Andreev, and Y. Koucheryavy, "Analysis of human body blockage in millimeter-wave wireless communications systems," in *IEEE International Conference on Communications (ICC)*, May 2016.
- [19] "5G channel model for bands up to 100 GHz," in *Workshop on Mobile Communications in Higher Frequency Bands, IEEE Globecom*, 2016. White paper.
- [20] M. Jacob, S. Priebe, A. Maltsev, A. Lomayev, V. Erceg, and T. Kurner, "A ray tracing based stochastic human blockage model for the IEEE 802.11ad 60 GHz channel model," in *Proc. of European Conference on Antennas and Propagation (EUCAP)*, April 2011.
- [21] G. MacCartney, S. Deng, S. Sun, and T. S. Rappaport, "Millimeter-Wave human blockage at 73 GHz with a simple double knife-edge diffraction model and extension for directional antennas," in *IEEE Vehicular Technology Conference (VTC Fall)*, September 2016.
- [22] K. Koufos and C. P. Dettmann, "Temporal correlation of interference in bounded mobile ad hoc networks with blockage," available at <https://arxiv.org/abs/1606.01840>, June 2016.
- [23] X. Zhang, F. Baccelli, and R. W. Heath Jr., "An indoor correlated shadowing model," in *IEEE Global Communications Conference (GLOBECOM)*, December 2015.
- [24] F. Baccelli and X. Zhang, "A correlated shadowing model for urban wireless networks," in *IEEE Conference on Computer Communications (INFOCOM)*, August 2015.
- [25] K. Mahler, W. Keusgen, F. Tufvesson, T. Zemen, and G. Caire, "Tracking of wideband multipath components in a vehicular communication scenario," *IEEE Transactions on Vehicular Technology*, March 2016.
- [26] S. Hahn, D. M. Rose, J. Sulak, and T. Kurner, "Impact of realistic pedestrian mobility modelling in the context of mobile network simulation scenarios," in *IEEE Vehicular Technology Conference (VTC Spring)*, May 2015.
- [27] A. Samuylov, M. Gapeyenko, D. Moltchanov, M. Gerasimenko, S. Singh, N. Himayat, S. Andreev, and Y. Koucheryavy, "Characterizing spatial correlation of blockage statistics in urban mmWave systems," in *IEEE Global Communications Workshops (GLOBECOM Wkshps)*, 2016.
- [28] P. Madadi, F. Baccelli, and G. Veciana, "On temporal variations in mobile user SNR with applications to perceived QoS," in *International Symposium on Modeling and Optimization in Mobile, Ad Hoc, and Wireless Networks (WiOpt)*, 2016.
- [29] M. Jacob, S. Priebe, T. Kurner, M. Peter, M. Wisotzki, R. Felbecker, and W. Keusgen, "Fundamental analyses of 60 GHz human blockage," in *European Conference on Antennas and Propagation (EuCAP)*, April 2013.
- [30] D. R. Cox and H. D. Miller, *The theory of stochastic processes*. Wiley, 1965.
- [31] D. R. Cox, *Renewal theory*. Methuen and Co Ltd., 1970.
- [32] D. Delay, "The busy period of the M/GI/∞ queue," *Queueing Systems: Theory and Applications*, vol. 38, no. 2, pp. 195–204, 2001.
- [33] S. Ross, *Introduction to probability models*. Academic Press, 10th ed., 2009.
- [34] J. Walrand and A. K. Parekh, "Congestion control, routing and scheduling in communication networks: A tutorial," *IEICE Transactions on Communications*, vol. 96, no. 11, pp. 2714–2723, 2013.
- [35] "WINTERSim system-level simulator, 2015," <http://winter-group.net/downloads/>.